Supplementary material: Improving the conductance of carbon nanotube networks through resonant momentum exchange

Robert A. Bell,[1] Michael C. Payne,[1] and Arash A. Mostofi[2]

[1] *Theory of Condensed Matter Group, Cavendish Laboratory, Cambridge, UK*
[2] *Departments of Materials and Physics, and the Thomas Young Centre for Theory and Simulation of Materials, Imperial College London, London SW7 2AZ, UK*

(Dated: May 21, 2014)

In this supplementary material, we provide additional details for several points mentioned in the main text.

I. RESONANT TUNNELLING IN COMPOSITIONALLY-DISORDERED METALLIC CNT NETWORKS

In the main text, we compare the inter-tube conductance for a system with no external potential to that with a resonant external potential for all metallic pairs of CNTs in the diameter range $1.2 - 1.6$ nm. Where both CNTs are chiral, we present results for CNTs with the opposite handedness. In Fig. S1, we present equivalent data where the two CNTs have the same handedness showing quantitatively equivalent results. In all cases, the inter-tube conductances are lower due to the greater registry mismatch between the two graphene lattices; for sufficient contact interaction length for incommensurate CNTs this relative handedness effect will diminish as the irrational unit cell length ratio removes any pseudo-alignment of the graphene lattices.

In Figs. S2 and S3 we present results for all pairs of metallic CNTs irrespective of relative handedness. In Fig. S2, we show the relative improvement in inter-tube conductance, defined as the ratio of the maximum improvement at resonance to the intrinsic inter-tube conductance, as a function of the difference in chiral angle. For CNTs with similar chiral angles, there is no improvement in the inter-tube conductance as energy-momentum-conserving tunnelling can occur at first-order, and hence the contribution is already large without an external potential. For CNTs with chiral angles differing by more than 3°, there is an improvement by up to two orders of magnitude due to the momentum-resonant external potential.

In Fig. S3 we compare the intrinsic inter-tube conductance (with $V_{\text{ext}} = 0$) to the maximum enhanced conductance. Where the intrinsic conductance is suppressed, there is a large improvement; for large intrinsic inter-tube conductances, the improvement is much smaller and is largely a result of resonant back-scattering (see below) and not a result of the second-order mechanism discussed in the main text.

In Fig. S4 we show a histogram of the momentum exchanges at resonance. For each CNT pair, we consider all peaks and not just that which gives the maximum improvement. Three histograms are shown giving the number of resonances in each momentum-exchange interval that improve the inter-tube conductance by a factor of at least 2, 5, and 10 respectively. As the resonant momentum-exchanges are distributed fairly evenly over the range considered we conclude that, to improve conductance between many different CNT pairs, the external potential should contain a wide selection of long-range Fourier components.

II. CHIRALITY HANDEDNESS DEPENDENCE OF RESONANT MOMENTUM EXCHANGES

Where both CNTs are chiral, the relative handedness of the CNTs may be the same or opposite. Chemically, the situations are identical as the densities of states are the same, as are the spatial distributions of the eigenstates (albeit with opposite handedness). The momentum-resonance mechanism predicts, however, that these two situations are different as the graphene Brillouin zones are rotated in the opposite(same) direction for opposite(same) handedness. This gives rise to different momentum differences between Dirac points, and hence different resonant momentum exchanges. This is confirmed in Fig. S5 where we show the inter-tube conductance at the Fermi energy as a function of momentum exchange for both relative handedness for the $(19, 1)/(14, 8)$ CNT pair, when they have the same and opposite handedness.

III. ENERGY DEPENDENCE OF INTER-TUBE SCATTERING

In the main text, we discuss the transmission spectrum as a function of energy in the presence of a resonant external potential. Indexing the leads as in Fig. 1 of the main text, transmission between leads 1 and 3 requires the coupling of states travelling forward in CNT 1, and backward in CNT 2, corresponding to coupling bands with opposite Fermi velocities.

In Fig. S6 we compare the transmission spectra with and without the external potential as a function of momentum exchange for a $(9, 0)/(5, 5)$ CNT pair. In the absence of the external potential, two peaks (with side lobes) exist at $\sim \pm 0.70$ eV, corresponding to energies where the two CNT dispersion relations cross. At these energies, momentum conserving tunnelling can occur at

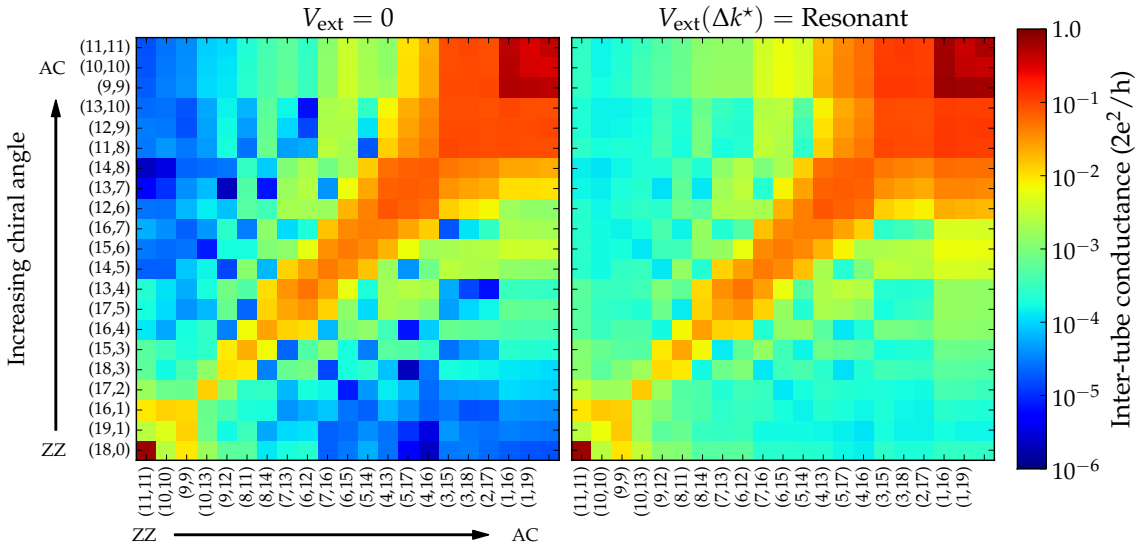

FIG. S1. As Fig. 3, with CNTs of same handedness. The inter-tube conductance between all pairs of metallic CNTs in the diameter range $1.2 - 1.6$ nm. Left: intrinsic conductance $V_{ext} = 0$; right: maximum enhanced conductance (V_{ext} resonant). The CNTs are ordered by increasing chiral angle and labelled by the (n, m) chiral indices.

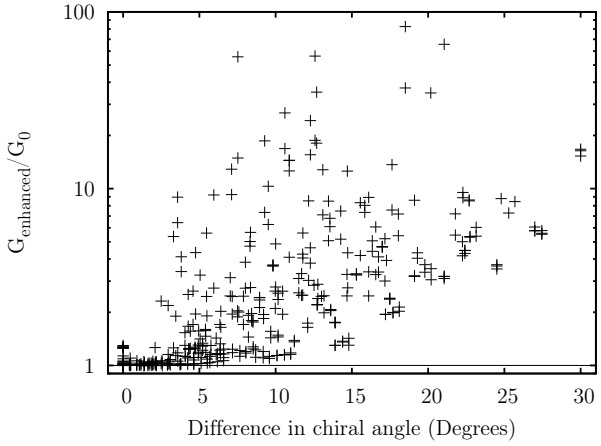

FIG. S2. The improvement in the inter-tube conductance as a function of the difference in CNT chiral angles. The improvement is defined as the ratio of the maximum inter-tube conductance when the external potential is at momentum resonance to the intrinsic conductance.

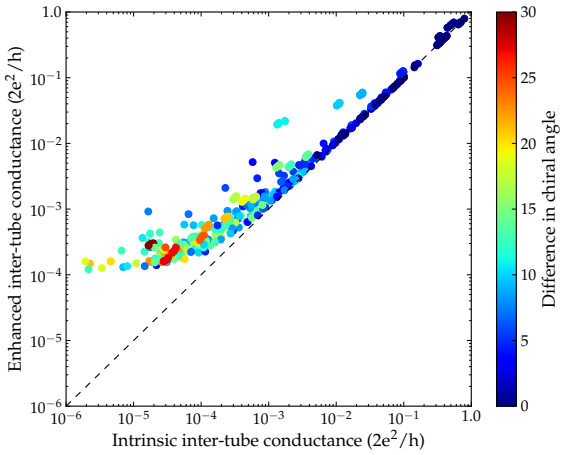

FIG. S3. A comparison of the inter-tube conductance at the Fermi energy. The intrinsic conductance is without external potential; the enhanced conductance is the maximum inter-tube conductance when the external potential is at momentum resonance. Points that lie above the dashed line represent CNT pairs in which the conductance is enhanced with respect to the intrinsic conductance. The points are colour-coded by the difference in CNT chiral angle.

first order, and conductance is not suppressed. This is discussed in Ref. 1. Due to the linear dispersion relations around the Fermi energy, for CNTs with different chiralities these peaks are guaranteed to lie away from the (un-doped) Fermi energy and will therefore generally not contribute to inter-tube conductance.

In the presence of an external potential that is sightly off-resonance, additional peaks appear in the transmission due to the second-order mechanism that we discuss in the main text. These peaks correspond to tunnelling between states that are separated by this momentum exchange, but do not lie at the Fermi energy, as indicated in the inset to Fig. S6. As the momentum exchange approaches resonance, these additional peaks move towards

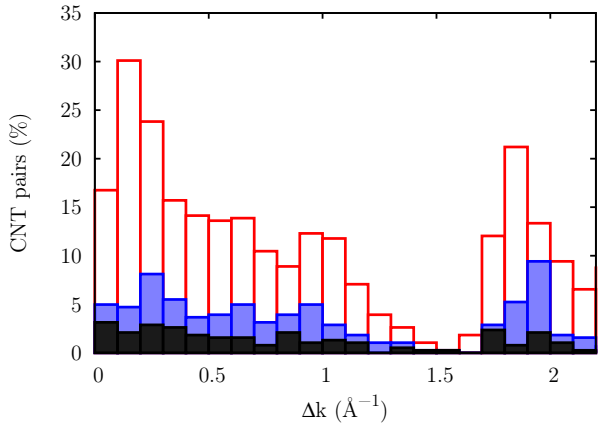

FIG. S4. The fraction of the 382 CNT pairs studied that have a given momentum resonance that increases inter-tube conductivity by a factor of at least: 2 (empty red), 5 (blue) and 10 (filled black).

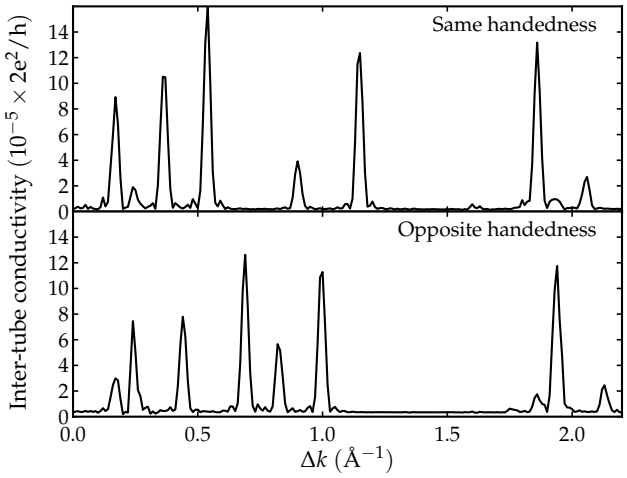

FIG. S5. The inter-tube conductance between the $(19, 1)/(14, 8)$ CNT pair as a function of momentum exchange. Top panel: same handedness; bottom panel: opposite handedness.

the Fermi energy.

IV. RESONANT BACK-SCATTERING

Back-scattering by potentials varying on length-scales larger than the carbon-carbon bond-length has been shown to be vanishing for metallic CNTs.[2] To put this into the context of this work, we consider the intra-tube conductance corresponding, for example, to transmission from lead 1 to lead 2 (Fig. 1). In Fig. S7 we show the intra-tube conductance at the Fermi energy as a function of momentum exchange for the $(18, 0)/(10, 10)$ CNT

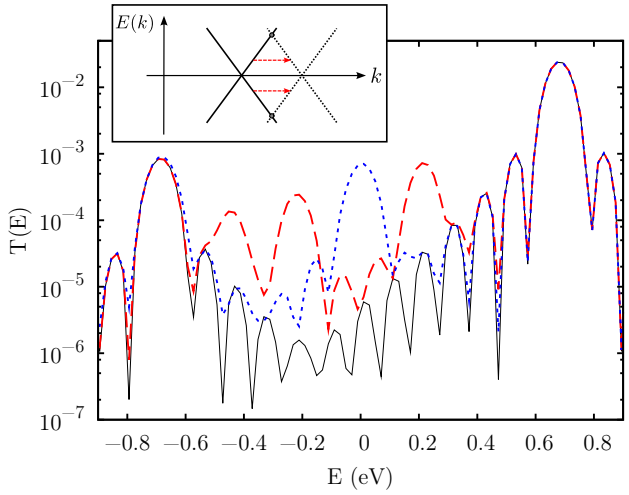

FIG. S6. Main: the transmission between leads 1 and 3 for the $(9, 0)/(5, 5)$ CNT pair as a function of electron energy for $\hat{V}_{\text{ext}} = 0$ (solid black), off-resonance $\Delta k = 0.78$ Å^{-1} (long-dashed red) and at resonance $\Delta k = 0.85$ Å^{-1} (short-dashed blue). The Fermi energy is zero. Inset: the projection of the dispersion relations onto the axial momentum axis. The states involved in scattering for $\Delta k = 0.78$ Å^{-1} are shown by the arrows.

pair. For most momentum exchanges, there is no noticeable decrease in transmission, in agreement with Ref. 2; for three momentum exchanges, sharp dips in the conductance appear. The momentum exchange of these features correspond precisely to the momentum difference between different Dirac points belonging to the same CNT. This is shown in the inset to Fig. S7. At these momentum exchanges, these states can mix causing strong back-scattering, greatly reducing the intra-tube conductance. As a result of this mixing and the local change in the conducting states/density of states, the inter-tube conductance may also be modified, as shown in Fig. S8. This improvement is not a consequence of the second order mechanism presented in the main text, but rather to the relative decrease in the intra-tube conductance as a result of back-scattering. Mixing between states away from the Fermi energy but at the same Dirac point is forbidden by the orthogonality of the subbands, preventing back-scattering for small momentum exchanges.

Scattering between states at the same Dirac point is not forbidden in semiconductor CNTs as the states belong to the same subband. Therefore, for small momentum exchanges, there is a strong intra-tube back-scattering as shown in Fig. S9.

Additional peaks exist for momentum exchanges larger than the maximum exchange Δk_{max} considered in the main text. These processes involve scattering between Dirac points outside the first graphene Brillouin zone. For incommensurate CNTs, these Dirac points are not equivalent to those in the principle Brillouin zone as the

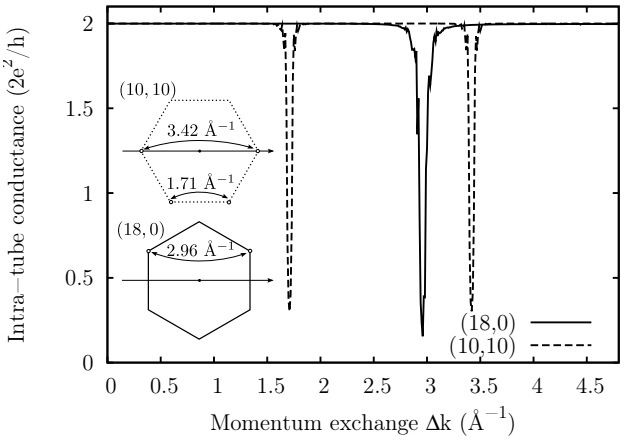

FIG. S7. The intra-tube conductance for the $(10, 10)/(18, 0)$ CNT pair. The inset shows the Dirac points involved in the resonant back-scattering processes.

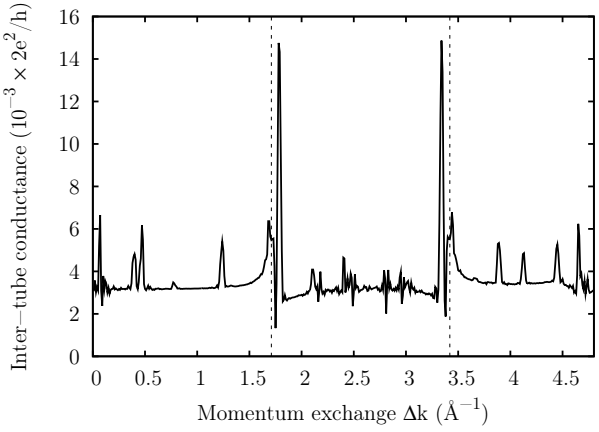

FIG. S8. The inter-tube conductance between the $(10, 10)/(13, 4)$ CNT pair. In addition to the peaks arising due to the second-order mechanism discussed in the main text, two additional peaks at $\Delta k \approx 1.7$ Å^{-1} and 3.4 Å^{-1} are present due to resonant back-scattering in the $(10, 10)$ CNT. The dashed lines give the positions of these back-scatterings. Although the improvement in the inter-tube conductance is greater here, the intra-tube conductance is strongly suppressed in the $(10, 10)$ CNT.

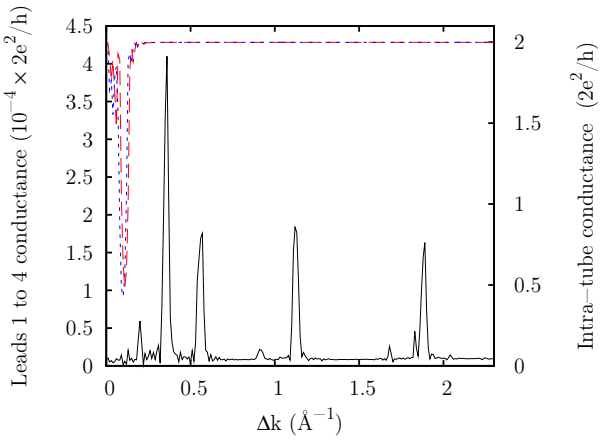

FIG. S9. Black line: the conductance between leads 1 and 4 at $E = 0.4$ eV for the $(20, 0)/(14, 7)$ CNT pair. Long-dash red/short-dash blue lines: intra-tube conductance for $(20, 0)$ and $(14, 7)$ CNTs.

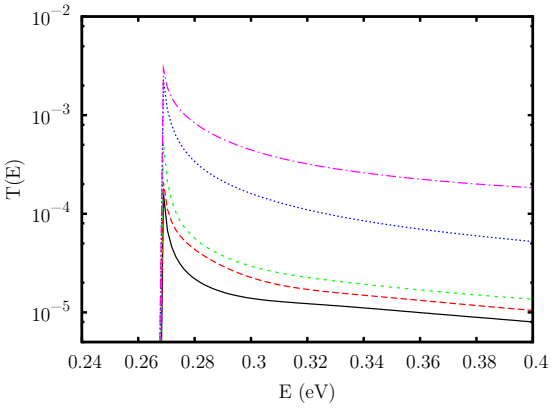

FIG. S10. The transmission spectrum between leads 1 and 4 for the $(20, 0)/(14, 7)$ CNT pair. Solid black line: $V_{\text{ext}} = 0$; dotted lines: Δk increasing from 1.06 Å^{-1} (long-dashed, red) to resonance at 1.12 Å^{-1} (dot-dashed, magenta) in steps of 0.02 Å^{-1}.

combined CNTs have no overall periodicity.

V. RESONANCE IN SEMICONDUCTOR CNTS

The momentum resonance occurs not only between metallic CNTs, but also semiconductor CNTs. In Fig. S9 we show the lead 1 to lead 4 inter-tube conductance between the $(20, 0)/(14, 7)$ CNT pair at $E = 0.4$ eV. The peaks in conductance correspond to momentum-resonant tunnelling. For semiconductor CNTs with similar diameter, the band gap and electron/hole effective masses are similar. Consequently, conduction/valence bands become aligned and the same momentum exchange can improve inter-tube conductance over a wide energy range. This is shown for transmission between leads 1 and 4 in Fig. S10. At the valence/conduction band edge, the improvement is further enhanced by the large density of states at the van Hove singularities.

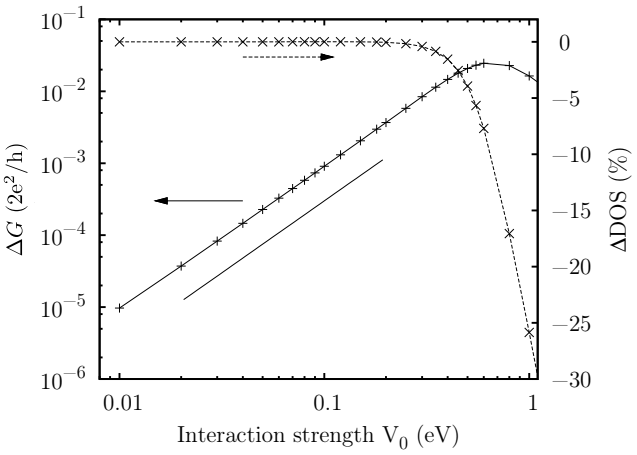

FIG. S11. Dependence of inter-tube conductance on external potential amplitude V_0. The CNT pair is $(9,0)/(5,5)$, with external potential at resonant momentum transfer $\Delta k = 0.85$ Å^{-1}. Shown is the additional conductance with the intrinsic contribution subtracted. The line segment corresponds to a quadratic dependence $\Delta G \sim V_0^2$. The change in the density of states (DOS) at the Fermi energy is also given as a percentage of the DOS at the Fermi level in the absence of the external potential.

VI. SCALING RELATIONS OF THE SCATTERING MECHANISM

The second-order momentum-resonant mechanism presented in Eqn. (4) in the main text is expected to follow specific scaling relations. Firstly, the scattering rate depends quadratically on the amplitude of the external potential V_0. This is indeed found to be the case as shown in Fig. S11. For sufficiently large interaction strength, scattering becomes non-perturbative and the inter-tube conductance greatly decreases. The density of states at the Fermi level is also strongly modified, resulting in increased back-scattering (not shown).

Secondly, the scattering rate depends on the square of the tunnelling matrix element, e.g. $\langle m|\hat{H}_T|\psi_2\rangle$. In Ref. 1, it was shown that this matrix element oscillates as a function of the contact region length L where momentum-conservation is not satisfied, a consequence of interference, and that at momentum resonance it grows linearly with L, giving a quadratic dependence on the inter-tube scattering rate.

Both these effects are observed, as shown in Fig. S12. Where momentum resonance is satisfied, the inter-tube conductance is a sum of the momentum-resonant second-order term that grows quadratically, and an oscillatory interference term due to the contribution arising at first order.

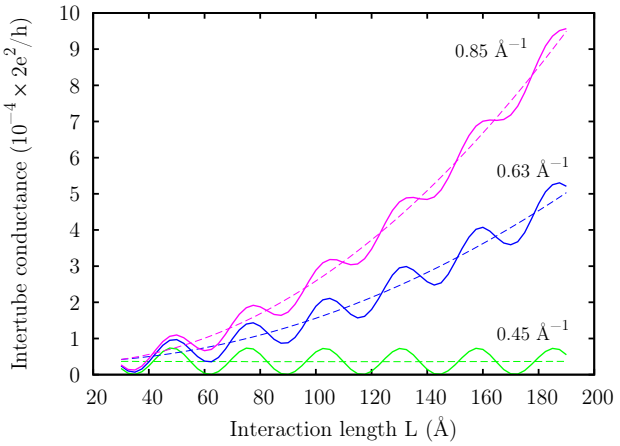

FIG. S12. The length dependence of the inter-tube conductance at the Fermi energy for $(9,0)/(5,5)$ CNT pair for three momentum transfers 0.45 Å^{-1}, 0.63 Å^{-1}, 0.85 Å^{-1}. For resonant momenta exchanges (0.63 Å^{-1}, 0.85 Å^{-1}), the conductance grows as the square of the interaction length $G \sim L^2$; away from resonance (0.45 Å^{-1}) the length dependence is oscillatory due to interference. The dotted lines give quadratic fits to the resonant curves to guide the eye.

VII. CALCULATING THE TRANSMISSION SPECTRUM

The transmission spectrum is calculated via a Green's function method.[3] The retarded Green's function at energy E is calculated via matrix inversion of the system Hamiltonian

$$G_r(E) = \big[(E + i\eta) - H - \Sigma\big]^{-1} \tag{S1}$$

with the semi-infinite leads taken into account through the self energies $\Sigma(E)$, calculated using the iterative approach of Lopez-Sancho *et al.*,[4] and η is an infinitesimal energy set at 3×10^{-6} eV. Instabilities at the Fermi energy are avoided by calculating the transmission at $E_F + 0.01$ eV.

The ballistic transmission probability from lead α to β is calculated using the Caroli formula

$$T_{\alpha\to\beta}(E) = \mathrm{tr}\big(\Gamma_\alpha G_r(E) \Gamma_\beta G_a(E)\big) \tag{S2}$$

with $\Gamma_\alpha = i(\Sigma_\alpha - \Sigma_\alpha^\dagger)$ and $G_a = G_r^\dagger$ the advanced Green's function.

The damping of the intrinsic interaction Hamiltonian and external potential are achieved using the damping function of Ref. 1:

$$t_{\alpha\beta} \to t(\mathbf{r}_\alpha, \mathbf{r}_\beta) \times f_d(z_\alpha; L, L_c) f_d(z_\beta; L, L_c) \tag{S3}$$

$$V_{\mathrm{ext}}(\mathbf{r}) \to V_{\mathrm{ext}}(\mathbf{r}) \times f_d(z; L, L_c) \tag{S4}$$

with

$$f_d(z; L, L_c) = \big[(e^{(z-L)/L_c} + 1)(e^{-z/L_c} + 1)\big]^{-1}. \tag{S5}$$

This introduces a contact length-scale L_c over which the intrinsic and external interactions activate. We choose $L_c = 5$ Å which is larger than the inter-tube separation (3.4 Å) and therefore is not the dominant source of momentum relaxation, and has negligible effect on the inter-tube conductance.[1]

A benefit of the second-order mechanism presented in the main text is that it does not need to modify the contact region of the CNTs. The model external potential used in the tight-binding calculations does not directly couple the CNTs, however it does exist within this contact region. We have verified that our conclusions do not change if the potential is present only in regions localised away from the contact region in the x-y plane, with the same periodic form along the axial z direction.

The form of the external potential used in the numerical model allows only axial momentum exchange. The azimuthal momentum difference between the Dirac points involved in scattering is not conserved as rotational symmetry is broken by the side-by-side geometry of the CNTs.

[1] M. A. Tunney and N. R. Cooper, Phys. Rev. B, **74**, 075406 (2006).
[2] T. Ando and T. Nakanishi, Journal of the Physical Society of Japan, **67**, 1704 (1998).
[3] S. Datta, *Electronic Transport in Mesoscopic Systems* (Cambridge University Press, 1995).
[4] M. P. L. Sancho, J. M. L. Sancho, and J. Rubio, Journal of Physics F: Metal Physics, **14**, 1205 (1984).